AIP | Applied Physics Letters

Realizing in-plane surface diffraction by x-ray multiple-beam diffraction with large incidence angle

Xian-Rong Huang, Ru-Wen Peng, Thomas Gog, D. P. Siddons, and Lahsen Assoufid

Citation: Applied Physics Letters **105**, 181903 (2014); doi: 10.1063/1.4901046
View online: http://dx.doi.org/10.1063/1.4901046
View Table of Contents: http://scitation.aip.org/content/aip/journal/apl/105/18?ver=pdfcov
Published by the AIP Publishing

Articles you may be interested in

The effect of specimen surface curvature on x-ray diffraction peak profiles
Rev. Sci. Instrum. **84**, 095105 (2013); 10.1063/1.4820444

Investigation of the near-surface structures of polar InN films by chemical-state-discriminated hard X-ray photoelectron diffraction
Appl. Phys. Lett. **102**, 031914 (2013); 10.1063/1.4789373

Growth and capping of InAs/GaAs quantum dots investigated by x-ray Bragg-surface diffraction
J. Appl. Phys. **105**, 036104 (2009); 10.1063/1.3074376

Time-resolved reflection surface x-ray diffraction
Rev. Sci. Instrum. **73**, 1720 (2002); 10.1063/1.1435823

High-resolution grazing-incidence x-ray diffraction for characterization of defects in crystal surface layers
J. Appl. Phys. **81**, 175 (1997); 10.1063/1.363838

This article is copyrighted as indicated in the article. Reuse of AIP content is subject to the terms at: http://scitation.aip.org/termsconditions. Downloaded to IP: 146.137.70.71 On: Wed, 05 Nov 2014 18:46:05

APPLIED PHYSICS LETTERS **105**, 181903 (2014)

Realizing in-plane surface diffraction by x-ray multiple-beam diffraction with large incidence angle

Xian-Rong Huang,[1,a)] Ru-Wen Peng,[2,b)] Thomas Gog,[1] D. P. Siddons,[3] and Lahsen Assoufid[1]
[1]*Advanced Photon Source, Argonne National Laboratory, Argonne, Illinois 60439, USA*
[2]*National Laboratory of Solid State Microstructures and Department of Physics, Nanjing University, Nanjing 210093, China*
[3]*National Synchrotron Light Source, Brookhaven National Laboratory, Upton, New York 11973, USA*

(Received 13 September 2014; accepted 21 October 2014; published online 4 November 2014)

Based on rigorous dynamical-theory calculations, we demonstrate the principle of an x-ray multiple-beam diffraction (MBD) scheme that overcomes the long-lasting difficulties of high-resolution in-plane diffraction from crystal surfaces. This scheme only utilizes symmetric reflection geometry with large incident angles but activates the out-of-plane and in-plane diffraction processes simultaneously and separately in the continuous MBD planes. The in-plane diffraction is realized by detoured MBD, where the intermediate diffracted waves propagate parallel to the surface, which corresponds to an absolute Bragg surface diffraction configuration that is extremely sensitive to surface structures. A series of MBD diffraction and imaging techniques may be developed from this principle to study surface/interface (misfit) strains, lateral nanostructures, and phase transitions of a wide range of (pseudo)cubic crystal structures, including ultrathin epitaxial films and multilayers, quantum dots, strain-engineered semiconductor or (multi)ferroic materials, etc. © *2014 AIP Publishing LLC*.
[http://dx.doi.org/10.1063/1.4901046]

X-ray diffraction is one of the most widely used techniques for characterization of crystalline materials with unrivalled angular resolution and strain sensitivity. However, since the interaction of x-rays with materials is a weak scattering process, x-ray diffraction usually requires a large crystal volume to collectively produce strong and sharp diffraction signals, which makes it difficult to use this technique to study ultrathin films and nanostructures. The other limitation is that the Bragg reflection geometry has very limited sensitivity to in-plane structures or strains (parallel to the surface). For example, the most commonly used symmetric reflection geometry can *only* detect the out-of-plane structures (along the surface normal direction), while the in-plane information, which is usually more critical for understanding misfit strains and relaxation, lateral nanostructure patterns, critical phenomena of surfaces and interfaces, etc, is lost.[1]

To overcome these limitations, researchers have made tremendous efforts to develop extremely asymmetric diffraction schemes, particularly grazing-incidence diffraction, to increase the in-plane sensitivity and reduce the x-ray penetration depth (so as to enhance surface or interface diffraction).[1–5] In addition to its experimental complexities, however, grazing-incidence diffraction unfortunately suffers from many severe difficulties, including (i) low diffraction efficiency (due to x-ray total external reflection), (ii) low angular resolution (associated with the broad diffuse grazing diffraction peaks), and (iii) extremely low spatial resolving resolution for surface mapping and imaging due to the large footprint of the grazing-incident beam on the sample. These drawbacks have significantly hindered the applications of high-resolution x-ray diffraction although more powerful x-ray sources, particularly modern synchrotrons with two-dimensional beam collimation,[6] are available or emerging.

Here, we present a simple scheme to solve the long-lasting difficulties of in-plane diffraction. It only utilizes the symmetric reflection geometry with large incident angles but can produce two individual diffraction peaks through the x-ray multiple-beam diffraction (MBD) effect. These two peaks correspond exactly to the out-of-plane and in-plane diffraction processes, respectively, such that the two kinds of structural information can be revealed simultaneously but independently. Although it involves no grazing incidence, the intermediate diffracted waves in the MBD process propagate almost exactly parallel to the surface. Therefore, this scheme is extremely sensitive to surface structures, and thus can be used to study and image a wide range of epitaxial (as well as bulk) materials, including ultrathin films and multilayers, quantum dots, nanowires, strain-engineered (multi)ferroic or electronic materials,[7–10] etc.

Si and GaAs in the (001) orientation provide the foundation for semiconductor microelectronics, so we focus on the simple symmetric 004 reflection from the (001) surface of a cubic crystal structure in Fig. 1(a). We will demonstrate that this routine configuration has a series of surprising diffraction properties.

For cubic crystal structures, a back reflection $\mathbf{g}_1 = HKL$ with Bragg angle θ_B close to 90° is usually accompanied by parasitic reflections $\mathbf{g}_m = hkl$ that fulfill the condition $h^2 + k^2 + l^2 = Hh + Kk + Ll$, and the parasitic reflections always form "conjugate pairs" ($\mathbf{g}_m$, $\mathbf{g}_{m'} = \mathbf{g}_1 - \mathbf{g}_m$).[11–13] For $\mathbf{g}_1 = 004$, this principle gives two parasitic reflection pairs (202, $\bar{2}02$) and (022, $0\bar{2}2$), with the corresponding reciprocal lattice points G_2, G_3, G_4, and G_5 all located on the equator of the 004 back-reflection Ewald sphere in Fig. 1(b), i.e., exact 004 back reflection is a six-beam diffraction configuration. Interestingly, the MBD can extend to a full continuous angular range of $0° < \theta \leq 90°$ along specific directions. In

a)Electronic address: xiahuang@aps.anl.gov
b)Electronic address: rwpeng@nju.edu.cn

 © 2014 AIP Publishing LLC

This article is copyrighted as indicated in the article. Reuse of AIP content is subject to the terms at: http://scitation.aip.org/termsconditions. Downloaded to IP: 146.137.70.71 On: Wed, 05 Nov 2014 18:46:05

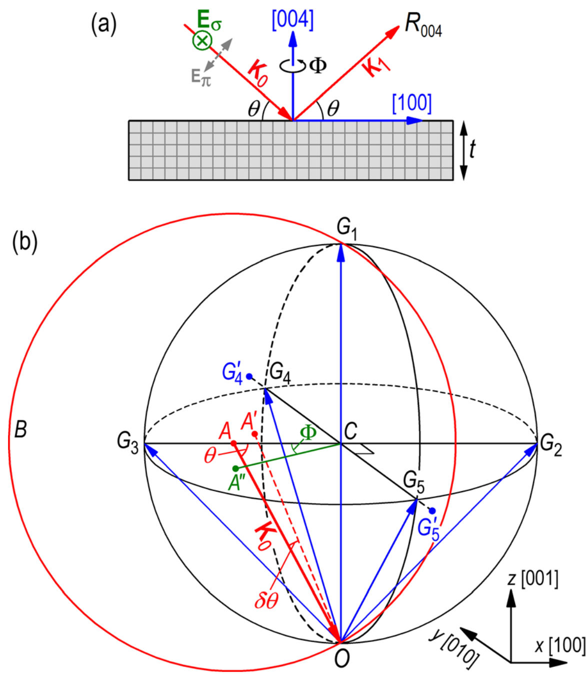

FIG. 1. (a) Symmetric 004 reflection geometry in real space for cubic structures. The plane of incidence is parallel to (010). $\mathbf{E}_\sigma$ and $\mathbf{E}_\pi$ indicate the σ- and π-polarization states of the electric fields. (b) MBD associated with 004 back reflection and its extension in reciprocal space. $O = 000$ is the origin of reciprocal space, and $C = 002$ is the back-reflection Ewald sphere center. The six diffraction vectors are $\mathbf{g}_0 = 000$ (forward transmission), $\mathbf{g}_1 = \overline{OG_1} = 004$ (primary reflection), $\mathbf{g}_2 = \overline{OG_2} = 202$, $\mathbf{g}_3 = \overline{OG_3} = \bar{2}02$, $\mathbf{g}_4 = \overline{OG_4} = 022$, and $\mathbf{g}_5 = \overline{OG_5} = 0\bar{2}2$.

Fig. 1(b), let us deviate the incident wavevector $\mathbf{K}_0$ from $\overline{CO}$(corresponding to the back-reflection condition) to $\overline{AO}$, where A is an arbitrary point on line G_2G_3 that is perpendicular to the circle $OG_4G_1G_5$ and passes through the circle center C. Obviously, A is always equidistance from O, G_4, G_1, and G_5, i.e., these points are also all located on a new Ewald sphere OG_1B centered at A, which corresponds to a four-beam diffraction configuration involving 004, 022, and $0\bar{2}2$ reflections. Hence, if the *plane of primary diffraction* (PPD) determined by $\mathbf{K}_0$ and $\mathbf{g}_1$ is the (010) lattice plane in Fig. 1(a), 004 reflection with Bragg wavelength $\boldsymbol{\lambda} = |AO|^{-1} = 2d\sin\boldsymbol{\theta}$ is always a four-beam diffraction process for any incidence angle, where θ is the incident angle and d is the spacing of the (004) Bragg planes. We call the (010) plane a *continuous MBD plane*. By symmetry, (100) is the other continuous MBD plane for 004, 202, and $\bar{2}02$ reflections.[14]

To verify this phenomenon, we have used the *Fourier coupled-wave diffraction theory* (FCWDT), which is a rigorous first-principles method,[15] to calculate the Si 004 four-beam Darwin curves for various incidence angles. Figure 2 shows four typical Darwin curves under the condition that the PPD is (010), where each four-beam diffraction peak splits into two subpeaks. Note that in Fig. 2(d), strong diffraction still occurs although the Bragg angle $\boldsymbol{\theta}_B = 45°$ makes the primary $000 \rightarrow 004$ reflection forbidden for π-polarization. As will be discussed below, the high 004 reflectivity here results from detoured diffraction. Above all, our calculations prove that strong MBD indeed occurs for all the Bragg angles of 004 reflection within the continuous MBD planes (010) and (100).

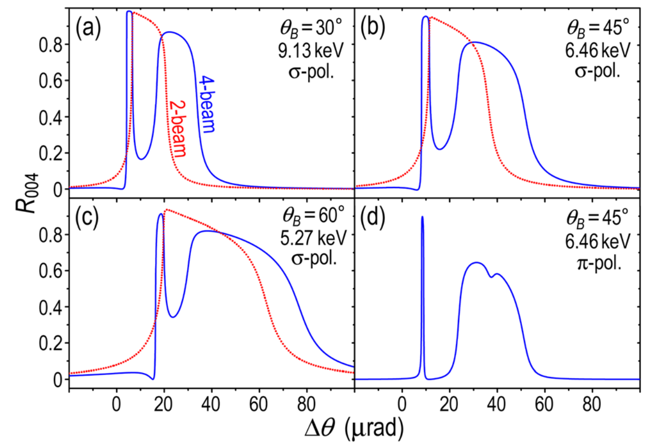

FIG. 2. Four-beam diffraction Darwin curves (in comparison with the regular two-beam Darwin curves) for different Bragg angles θ_B of symmetric Si 004 reflection within the (010) plane. $t = \infty$ and $\Phi = 0$.

Under the $000/004/022/0\bar{2}2$ four-beam diffraction condition, there exist three diffraction channels in Fig. 1(b) that contribute to the overall 004 reflection. The first one is the direct $000 \rightarrow 004$ channel, corresponding to the diffraction path $\overline{AO} + \overline{OG_1} = \overline{AG_1}$ or $\mathbf{K}_0 + \mathbf{g}_1 = \mathbf{K}_1$, where $\mathbf{K}_1 = \overline{AG_1}$ is the wavevector of the overall 004 reflection wave [see Fig. 1(a)]. The other channels are two detoured channels $000 \rightarrow 022 \rightarrow 0\bar{2}2$ and $000 \rightarrow 0\bar{2}2 \rightarrow 022$, which correspond to the diffraction paths $\overline{AO} + \overline{OG_4} + \overline{G_4G_1} = \overline{AG_1}$ $(\mathbf{K}_0 + \mathbf{g}_4 + \mathbf{g}_5 = \mathbf{K}_1)$ and $\overline{AO} + \overline{OG_5} + \overline{G_5G_1} = \overline{AG_1}$ $(\mathbf{K}_0 + \mathbf{g}_5 + \mathbf{g}_4 = \mathbf{K}_1)$, respectively, in Fig. 1(b). Here, note that $\mathbf{g}_4 + \mathbf{g}_5 = \mathbf{g}_1$, $\mathbf{g}_4 = \overline{OG_4} = \overline{G_5G_1}$, and $\mathbf{g}_5 = \overline{OG_5} = \overline{G_4G_1}$.

In the two detoured channels, the intermediate diffracted wavevectors are $\mathbf{K}_4 = \overline{AG_4}$ and $\mathbf{K}_5 = \overline{AG_5}$, respectively, which are parallel to the (001) crystal surface for symmetric 004 reflection. Therefore, $000 \rightarrow 022$ and $000 \rightarrow 0\bar{2}2$ are the so-called *Bragg surface diffraction*[13,16] with the diffracted waves propagating parallel to the surface. A unique property of Bragg surface diffraction is its ultrahigh surface sensitivity (corresponding to extremely small x-ray penetration). Here, for Si 004 four-beam diffraction, this property is demonstrated by the two Darwin curves of thin crystals in Fig. 3(a), where the reflectivity maxima for crystal thicknesses $t = 100$ and 50 nm are surprisingly high, $R_{004}^{\max} = 0.33$ and 0.032, respectively. In comparison, the corresponding reflectivity maxima of two-beam 004 reflection at the same Bragg angle $\boldsymbol{\theta}_B = 20°$ are only 7.6×10^{-4} [Fig. 4(b)] and 1.9×10^{-4} (not shown), respectively. In addition, the two-beam diffraction peak for $t = 50$ nm is quite diffuse (about 0.9 mrad wide) with satellite fringes, compared with the sharp peak in Fig. 3(a) that is only 1.6 μrad wide.

In Fig. 1(b), the Bragg conditions for 004, 022, and $0\bar{2}2$ are geometrically satisfied simultaneously when A is located on the line G_2G_3. But in reality, the Bragg peak of each reflection is always slightly shifted from the geometrical Bragg angle due to the small x-ray refraction. Here by symmetry, the refraction corrections of 022 and $0\bar{2}2$ are the same, but they are slightly different from that of 004. This difference causes the split of the four-beam 004 Bragg peak into two peaks in Figs. 2 and 3(a) for $t = \infty$. The left peak

This article is copyrighted as indicated in the article. Reuse of AIP content is subject to the terms at: http://scitation.aip.org/termsconditions. Downloaded to IP: 146.137.70.71 On: Wed, 05 Nov 2014 18:46:05

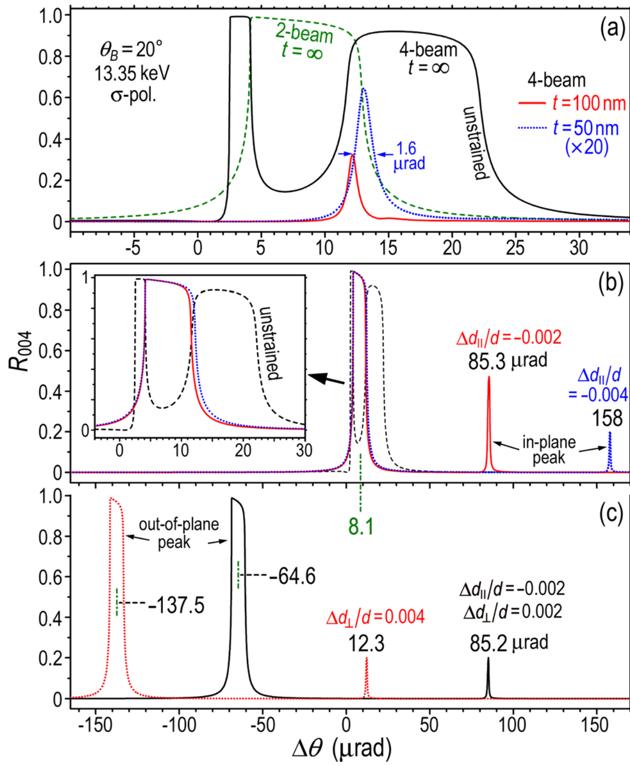

FIG. 3. (a) Si 004 diffraction Darwin curves calculated for different crystal thicknesses t. The sharp peaks for $t = 100$ and 50 nm are, in fact, the in-plane peaks. (b) Variation of 004 four-beam diffraction Darwin curves with in-plane strains. (c) Variation of the out-of-plane peak with out-of-plane strains. All the curves in (b) and (c) are based on $t = \infty$. $\Phi = 0$.

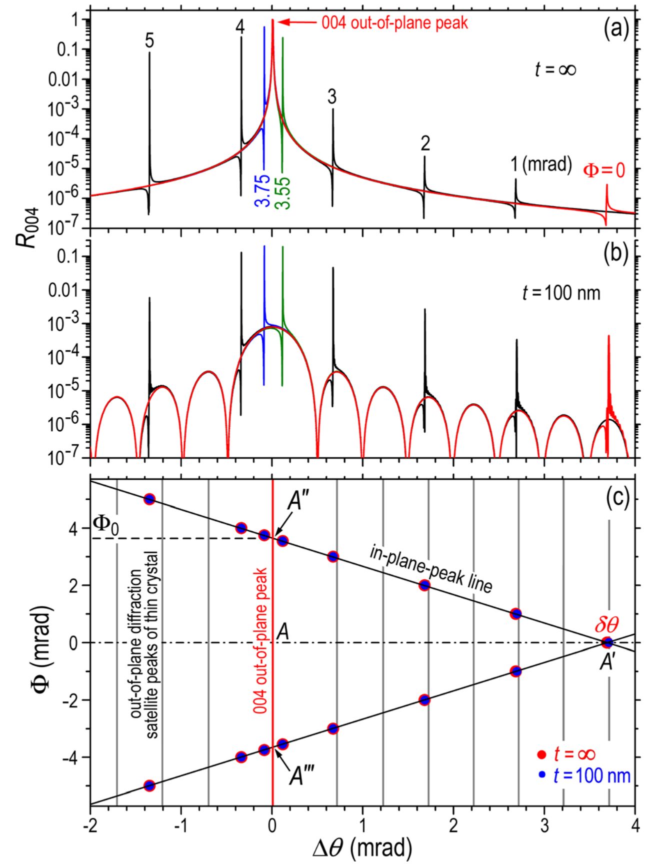

FIG. 4. Φ-dependent θ-scan diffraction patterns of Si 004 reflection, $\Delta d_{||}/d = -0.01$, and σ-polarization. (a) Diffraction from a semi-infinite crystal. (b) Diffraction from a thin crystal. (c) $\theta - \Phi$ mapping of the diffraction peaks in (a) and (b). Note that the out-of-plane peak and the diffraction fringes (for $t = 100$ nm) are invariant with Φ within a small Φ-range. Such features form the common "background" of all the related curves in (a) or (b). See Fig. 1(b) for the diffraction conditions of A, A', and A'' in reciprocal space.

corresponds to the direct $000 \rightarrow 004$ channel, while the right peak corresponds to the two detoured channels.

To prove this principle, we artificially induce a small homogeneous in-plane strain $\Delta d_{||}/d = -0.002$ to the semi-infinite crystal (while the out-of-plane lattice constant is unchanged). Compared with the unstrained crystal, this strain leads to two major changes in the overall 004 diffraction pattern in Fig. 3(b): (i) The right peak shifts significantly to $\Delta\boldsymbol{\theta}_{||} = 85.3\,\mu$rad and (ii) the left peak has a much smaller shift but with both its position and shape approaching those of the two-beam 004 Bragg peak in Fig. 3(a). When the strain is increased to $\Delta d_{||}/d = -0.004$, the left peak almost stops varying but the right peak shifts further to $\Delta\boldsymbol{\theta}_{||} = 158\,\mu$rad. For further increase of $\Delta d_{||}/d$, our FCWDT calculations show that the left peak becomes exactly the two-beam Darwin peak with the peak center fixed at $\Delta\boldsymbol{\theta}_0^{\perp} = 8.1\,\mu$rad. In comparison, the right peak keeps shifting and its peak center $\Delta\theta_{||}$ rigorously follows the equation:

$$\Delta d_{||}/d = -(\Delta\boldsymbol{\theta}_{||} - \Delta\boldsymbol{\theta}_0^{||})\cot\boldsymbol{\theta}_B, \tag{1}$$

where $\Delta\boldsymbol{\theta}_0^{||} = 12.3\,\mu$rad and θ_B (=20° here) is the 004 reflection Bragg angle. Obviously, Eq. (1) is the differential form of the in-plane Bragg equation $2d_{||}\sin\boldsymbol{\theta} = \boldsymbol{\lambda}$, where $d_{||}(= d + \Delta d_{||})$ is the spacing of the lateral (040) Bragg planes. Thus, it becomes clear that the right peak (here called the *in-plane peak*) indeed corresponds to an in-plane diffraction process that is the net effect of the two detoured diffraction channels $000 \rightarrow 022 \rightarrow 0\bar{2}2$ and $000 \rightarrow 0\bar{2}2 \rightarrow 022$. However, it should be noted that here θ is measured along the out-of-plane diffraction direction [see Fig. 1(a)], i.e., the in-plane diffraction is revealed along the 004 out-of-plane diffraction direction.

For comparison, now we induce an out-of-plane strain $\Delta d_{\perp}/d = 0.004$ to the crystal (with $\Delta d_{||} = 0$), which remarkably shifts the left peak from $\Delta\boldsymbol{\theta}_0^{\perp} = 8.1\,\mu$rad to $\Delta\boldsymbol{\theta}_{\perp} = -137.5\,\mu$rad in Fig. 3(c). In contrast, without the interaction of the left peak and the influence of in-plane strains, the in-plane peak is (always) located at $\Delta\boldsymbol{\theta}_0^{||} = 12.3\,\mu$rad, which is consistent with Eq. (1). Thus, $\Delta\boldsymbol{\theta}_0^{||}$ is the refraction correction to the in-plane diffraction. Obviously, the shift of the left peak (called the *out-of-plane peak*) satisfies the differential Bragg equation of the out-of-plane two-beam 004 reflection

$$\Delta d_{\perp}/d = -(\Delta\boldsymbol{\theta}_{\perp} - \Delta\boldsymbol{\theta}_0^{\perp})\cot\boldsymbol{\theta}_B, \tag{2}$$

where $\Delta\boldsymbol{\theta}_0^{\perp} = 8.1\,\mu$rad is the corresponding refraction correction. Therefore, we have proved that the two peaks in the four-beam 004 reflection are indeed independently caused by the out-of-plane and in-plane diffraction processes, respectively. The independence of the two peaks for strained crystals can be further proved by the diffraction pattern in Fig. 3(c) calculated with an out-of-plane strain $\Delta d_{\perp}/d = 0.002$ and an in-plane strain $\Delta d_{||}/d = -0.002$ applied simultaneously,

This article is copyrighted as indicated in the article. Reuse of AIP content is subject to the terms at: http://scitation.aip.org/termsconditions. Downloaded to IP: 146.137.70.71 On: Wed, 05 Nov 2014 18:46:05

where the two peaks shift simultaneously but independently according to Eqs. (1) and (2), respectively.

Understanding of Eq. (1) requires detailed analyses of Fig. 1(b). When the crystal has an in-plane strain $\Delta d_{||}/d$, the reciprocal lattice points G_4 and G_5 move away from the Ewald sphere OG_1B to $G_4{}'$ $(0, [2(d+\Delta d_{||})]^{-1}, (2d)^{-1})$ and $G_5{}'$ $(0, -[2(d+\Delta d_{||})]^{-1}, (2d)^{-1})$, respectively. (If the in-plane strain is isotropic, G_2 and G_3 will also shift.) Consequently, the incident wavevector $\mathbf{K}_0 = \overline{AO}$ only satisfies the Bragg condition of the direct 004 reflection ($\mathbf{g}_1 = \overline{OG_1}$), which gives rise to the out-of-plane peak in Fig. 3(b). To satisfy the Bragg conditions of 022 and $0\bar{2}2$, $\mathbf{K}_0$ must be rotated by $\delta\theta$ in the $OG_2G_1G_3$ plane [i.e., A moves to A' $(-\cos(\boldsymbol{\theta}+\boldsymbol{\delta\theta})/\boldsymbol{\lambda}, 0, \sin(\boldsymbol{\theta}+\boldsymbol{\delta\theta})/\lambda)$] such that the condition $|A'G_4'| = |A'G_5'| = \lambda^{-1}$ is fulfilled. Based on $\lambda = 2d\sin\boldsymbol{\theta}$, one can prove that $|A'G_4'| = |A'G_5'| = \lambda^{-1}$ indeed leads to $\Delta d_{||}/d = -\boldsymbol{\delta\theta}\cot\boldsymbol{\theta}$, which is consistent with Eq. (1) except that the small refraction correction is not taken into account here. Note that under this condition, the Bragg condition of 004 reflection is not satisfied ($|A'G_1| \neq \lambda^{-1}$). Consequently, the Bragg peak corresponding to $\mathbf{K}_0 = \overline{A'O}$ is the pure in-plane diffraction peak.

In Fig. 3(b), the reflectivity of the in-plane peak drops quickly with increasing $\Delta d_{||}/d$, which is caused by the increasing deviation of the in-plane diffraction from the MBD condition. A simple way to solve this problem is to rotate the incident wavevector $\mathbf{K}_0$ in Fig. 1(b) by a small azimuthal angle Φ but with the tail of $\mathbf{K}_0$ remaining on the $G_2G_3G_4G_5$ plane. Apparently, there exists a point A'' on plane $G_2G_3G_4G_5$ that satisfies $|A''O| = |A''G_1| = |A''G_5'| = |\mathbf{K}_0| = 1/\lambda$. Under this condition, both the Bragg conditions of 004 reflection and the detoured $000 \to 0\bar{2}2 \to 022$ $(\overline{AO} + \overline{OG_5} + \overline{G_5G_1} = \overline{AG_1})$ channel are satisfied such that both diffraction processes are strongly activated. It can be proved that the azimuthal angle of A'' is simply $\Phi_0 = \boldsymbol{\delta\theta} \approx (\Delta d_{||}/d)\tan\boldsymbol{\theta}_B$ (with the small refraction correction ignored). [There exists a symmetric point A''' $(\Phi_0 = -\boldsymbol{\delta\theta})$ on plane $G_2G_3G_4G_5$ that satisfies the Bragg conditions of 004 reflection and the other detoured channel $000 \to 022 \to 0\bar{2}2$, see Fig. 4(c).] Thus, if one performs θ-scans with Φ close to Φ_0, the in-plane peak can be significantly enhanced even for highly strained crystals. This can be clearly seen from the FCWDT calculations in Fig. 4(a), where the in-plane peak reflectivity in the θ-scan diffraction patterns steadily increases when Φ increases towards $\Phi_0 = 3.63$ mrad. For example, the in-plane reflectivity maxima reach 0.25 and 0.57 for $\Phi_0 = 3.55$ and 3.75 mrad, respectively.

Figure 4(b) shows the corresponding θ-scan reflectivity curves for a thin Si crystal ($t = 100$ nm). As expected, the common out-of-plane peak in Fig. 4(a) becomes an extended diffuse peak surrounded by thickness fringes. In contrast, the in-plane peaks remain extremely sharp. Overall, the variation of the in-plane peak reflectivity with Φ follows the same trend as that in Fig. 4(a) and the peak positions remain nearly unchanged.[17]

Figure 4(c) is the $\boldsymbol{\theta} - \Phi$ map showing the positions of the diffraction peaks in Figs. 4(a) and 4(b). Here, the slopes of the two "in-plane-peak lines" are exactly ± 1, which proves $\Phi_0 = \boldsymbol{\delta\theta}$. The dependence of the θ-scan curves on Φ indicates that in experiments, two-dimensional $\boldsymbol{\theta} - \Phi$ mapping is required to precisely determine the $\Phi = 0$ reference line in Fig. 4(c). Afterwards, one may make a full θ-scan at $\Phi = 0$ to find the in-plane peak position $\delta\theta$ at A' so as to obtain $\Delta d_{||}/d$ from Eq. (1). For highly strained crystals, the in-plane peak at A' $(\boldsymbol{\delta\theta}, \Phi = 0)$ may be too weak to measure, but one may extrapolate the two in-plane-peak lines in Fig. 4(c), which always have strong diffraction intensities near A'' and A''' to A'. For a single pseudo-cubic crystal, $\Delta d_{||}/d$ represents the difference between the in-plane and out-of-plane lattice constants, from which one can derive the strains or deformations (self reference). For an epitaxial film on a substrate, the θ-Φ scan can simultaneously reveal the diffraction patterns of the substrate and epilayer, where the difference between the two in-plane Bragg angles precisely determines the in-plane misfit strains.[18]

In the above, we have assumed that the lateral dimensions of the crystals are homogeneously infinite, which makes the in-plane diffraction peaks extremely sharp even for ultrathin crystals. If the crystal has lateral modulations or patterns (such as quantum dots and wires), the in-plane peak will also show diffraction fringes or other patterns, similar to the out-of-plane diffraction patterns of layered structures. Therefore, this scheme is also capable of revealing lateral nanostructures on crystal substrates.

In summary, we have demonstrated the principles of a simple MBD scheme that can revolutionarily achieve pure high-resolution in-plane surface diffraction. It can be realized using both synchrotron and laboratory x-ray sources at any wavelengths. The only extra requirements are the high-precision Φ-rotation and a highly collimated incident beam along both the θ and Φ directions (typically $<20\,\mu$rad).[19] This scheme can be used for precise measurements of the strain states (including Poisson's ratios) of cubic-structure crystals without the need of references. It is also powerful for studying phase transitions between cubic and pseudocubic structures of a variety of (multi)ferroic materials.[7–10] For epitaxial systems, the θ-Φ scan can determine the absolute in-plane misfit strains and lateral nanostructures. Since it does not involve grazing incidence, the current scheme can also achieve high spatial resolution, based on which one may perform MBD x-ray topography[20] or micron-beam mapping to image the in-plane structures and defects (e.g., misfit dislocations or domains). Finally, since the continuous MBD mechanism can be activated at any wavelengths, it is also possible to combine this technique with resonant X-ray scattering.[21,22]

This work was supported by the U.S. Department of Energy, Office of Science, Office of Basic Energy Sciences, under Contract Nos. DE-AC02-06CH11357 and DEAC-02-98CH10886. R.-W.P. was supported by the MOST of China (Grant Nos. 2012CB921502 and 2010CB630705) and the NSFC (Grant Nos. 11034005, 61475070, and 91321312).

[1] U. Pietsch, V. Holý, and T. Baumbach, *High-Resolution X-ray Scattering: From Thin Films to Lateral Nanostructures* (Springer, Berlin, 2004).
[2] S. A. Stepanov, E. A. Kondrashkina, R. Köhler, D. V. Novikov, G. Materlik, and S. M. Durbin, Phys. Rev. B **57**, 4829 (1998).
[3] O. Thomas, Q. Shen, P. Schieffer, N. Tournerie, and B. Lépine, Phys. Rev. Lett. **90**, 017205 (2003).
[4] D. K. Bowen and B. K. Tanner, *X-Ray Metrology in Semiconductor Manufacturing* (CRC Press, Boca Raton, 2006).

This article is copyrighted as indicated in the article. Reuse of AIP content is subject to the terms at: http://scitation.aip.org/termsconditions. Downloaded to IP: 146.137.70.71 On: Wed, 05 Nov 2014 18:46:05

[5]K. Omote, J. Phys.: Condens. Matter. **22**, 474004 (2010).
[6]Two-dimensional collimation of the x-ray beam is the key requirement for MBD. Modern X-ray free-electron lasers and diffraction-limited storage rings based on multi-bend achromat (MBA) technology [E. A. Reich, Nature (London) **501**, 148 (2013)] can provide such naturally collimated beams.
[7]J. H. Lee, L. Fang, E. Vlahos, X. Ke, Y. W. Jung, L. F. Kourkoutis, J.-W. Kim, P. J. Ryan, T. Heeg, M. Roeckerath *et al.*, Nature (London) **466**, 954 (2010).
[8]J. Fujioka, Y. Yamasaki, H. Nakao, R. Kumai, Y. Murakami, M. Nakamura, M. Kawasaki, and Y. Tokura, Phys. Rev. Lett. **111**, 027206 (2013).
[9]F. Sandiumenge, J. Santiso, L. Balcells, Z. Konstantinovic, J. Roqueta, A. Pomar, J. P. Espinós, and B. Martínez, Phys. Rev. Lett. **110**, 107206 (2013).
[10]M. V. Holt, S. O. Hruszkewycz, C. E. Murray, J. R. Holt, D. M. Paskiewicz, and P. H. Fuoss, Phys. Rev. Lett. **112**, 165502 (2014).
[11]J. P. Sutter, E. E. Alp, M. Y. Hu, P. L. Lee, H. Sinn, W. Sturhahn, T. S. Toellner, G. Bortel, and R. Colella, Phys. Rev. B **63**, 094111 (2001).
[12]S.-L. Chang, Yu. P. Stetsko, M.-T. Tang, Y.-R. Lee, W.-H. Sun, M. Yabashi, and T. Ishikawa, Phys. Rev. Lett. **94**, 174801 (2005).
[13]S.-L. Chang, *X-ray Multiple-Wave Diffraction: Theory and Applications* (Springer, Berlin, 2004).
[14]Except 111 and 220, all Bragg reflections of cubic diamond structures have a series of continuous MBD planes. The surface normal to each continuous MBD plane is parallel to $\mathbf{g}_1 \times (\mathbf{g}_1 \times \mathbf{g}_m)$, where $\mathbf{g}_1 = HKL$ is the primary reflection, and the corresponding parasitic reflection pairs are $\mathbf{g}_m = hkl$ and $\mathbf{g}_{m'} = \mathbf{g}_1 - \mathbf{g}_m$ with $h^2 + k^2 + l^2 = Hh + Kk + Ll$. General cubic structures with less or no forbidden reflections have more continuous MBD planes. See X.-R. Huang, Q. Jia, M. Wieczorek, and L. Assoufid, J. Appl. Crystallogr. **47**, 1716 (2014).
[15]X.-R. Huang, R.-W. Peng, M. G. Hönnicke, and T. Gog, Phys. Rev. A **87**, 063828 (2013).
[16]R. Lang, A. S. de Menezes, A. O. dos Santos, S. Reboh, E. A. Meneses, L. Amarald, and L. P. Cardoso, J. Appl. Crystallogr. **46**, 1796 (2013).
[17]The right three in-plane peaks in Fig. 4(b) are about two-order higher than those in Fig. 4(a) because the 004 Bragg condition of the thin crystal is much less stringent due to the extended diffraction angular range. Thus, this scheme is very powerful for studying ultrathin crystal films (to a few nanometers).
[18]The fact that reflection 004 has two equivalent continuous four-beam diffraction planes (010) and (100) make it convenient to reveal strain or structural anisotropy by two sets of measurements within these two perpendicular planes, respectively.[3]
[19]For synchrotron X-ray beams with only natural vertical collimation ($\sim$10 μrad), the horizontal collimation can be achieved by simply using four-bounce horizontal diffraction monochromators. The emerging "ultimate" storage ring with multi-bend achromat lattice[6] may make high-resolution MBD revolutionarily powerful as the extremely bright X-ray beams will have two-dimensional ultrahigh collimation naturally.
[20]X. R. Huang, D. R. Black, A. T. Macrandera, J. Maj, Y. Chen, and M. Dudley, Appl. Phys. Lett. **91**, 231903 (2007).
[21]A. Frano, E. Schierle, M. W. Haverkort, Y. Lu, M. Wu, S. Blanco-Canosa, U. Nwankwo, A. V. Boris, P. Wochner, G. Cristiani *et al.*, Phys. Rev. Lett. **111**, 106804 (2013).
[22]A. Lupascu, J. P. Clancy, H. Gretarsson, Z. Nie, J. Nichols, J. Terzic, G. Cao, S. S. A. Seo, Z. Islam, M. H. Upton *et al.*, Phys. Rev. Lett. **112**, 147201 (2014).

This article is copyrighted as indicated in the article. Reuse of AIP content is subject to the terms at: http://scitation.aip.org/termsconditions. Downloaded to IP: 146.137.70.71 On: Wed, 05 Nov 2014 18:46:05